Scientific Journals
of the Maritime University of Szczecin

Zeszyty Naukowe
Akademii Morskiej w Szczecinie

2019, 60 (132), 192–199
ISSN 1733-8670 (Printed)
ISSN 2392-0378 (Online)
DOI: 10.17402/389

Received: 31.10.2019
Accepted: 28.11.2019
Published: 18.12.2019

Laboratory tests of a car seat suspension system equipped with an electrically controlled damper

Andrzej Zuska[1], Dariusz Więckowski[2]

[1] Kielce University of Technology, Faculty of Mechatronics and Mechanical Engineering
7 Tysiąclecia Państwa Polskiego Ave., 25-314 Kielce, Poland
e-mail: a.zuska@tu.kielce.pl
[2] Automotive Industry Institute
e-mail: d.więckowski@pimot.eu
corresponding author

Key words: acceleration, passive safety, road safety, vehicle safety, vibrational comfort, vibrations

Abstract

The paper presents the results of laboratory simulation tests of a suspension system for a car seat. The first part of the paper contains a description of the experiment, paying particular attention to the conditions in which the tests were conducted and the properties of the electrically controlled damper, which was mounted in the tested car seat's suspension. Graphs of the damper's operation were determined for different values of current intensity and the signal controlling the damper's damping ratio and then the damping characteristics were determined on this basis. Simulated tests of the car seat's suspension were carried out on a car component test station. During the tests, the values measured were the acceleration recorded at selected points on the dummy, which was placed on a seat equipped with suspension using a magnetorheological (MR) damper during the experiment. The second part of the paper presents an analysis of the results of the experimental tests with particular emphasis on the influence of the current that controls the operation of the damper on the values of the RMS index of the acceleration at selected points of the dummy.

Introduction

Semi-active suspension systems are a compromise between the effectiveness of vibration reduction and energy consumption. The operation of semi-active vibration isolation systems is based on modifying the damping and stiffness coefficients during the vibration cycle. For this purpose, actuators with adjustable damping and stiffness coefficients are used. It is becoming increasingly common for these elements to be designed with the use of smart materials, such as piezoelectrics, shape-memory materials, and magnetorheological fluids (Gromadowski, Osiecki & Stępiński, 1992; Gromadowski, Osiecki & Stępiński, 2001; Islam, Ahn & Truong, 2009; Truong & Ahn, 2012). Nowadays, controlled dampers that use magnetorheological and electrorheological fluids can be found in the offerings of a number of companies, and magnetorheological dampers are becoming more common in the automotive industry. There are many strategies for controlling the damping coefficients, the most common control methods include: SkyHook, GroundHook, and "clipped" LQR (Rakheja & Boileau, 1998; Islam, Ahn, & Truong, 2009; Truong & Ahn, 2012; Wu et al., 2018).

The principle of the operation of magnetorheological dampers (Islam, Ahn &Truong, 2009; Truong & Ahn, 2012; Jaśkiewicz & Więckowski, 2018) is based on a damper filled with a magnetorheological fluid, which is a combination of ferromagnetic filings and synthetic oil as the carrier fluid. A solenoid coil is placed in the piston of the damper, to which the current signal that controls the damper is supplied. The magnetic field lines that are generated by the coil envelop the MR fluid within the gap through which the MR fluid flows. The volume flow rate of the fluid between the damper chambers depends on the pressure difference in the

fluid chambers. The pressure difference is proportional to the forces acting on the individual columns of the MR damper. When there is no current in the coil, the ferromagnetic particles are dispersed in the carrier fluid and the MR damper behaves like a normal viscous damper. The movement of the piston is counteracted by the friction force in the seals and the force resulting from the flow of the fluid. If current is passed through the coil of the damper, the ferromagnetic particles are aligned parallel to the direction of the magnetic field (perpendicular to the direction of the fluid flow). The movement of the piston is also counteracted by the force of the magnetoresistance effect; the essence of this effect is that a change in the viscosity of the fluid in the working chamber can occur in mere milliseconds, as a result of the changes in the magnetic field.

As a result of changes in the viscosity, the flow of fluid through the gap is limited, which increases the hydraulic resistance of the movement of the piston and generates a damping force that corresponds to these changes. The control range of this force is limited by the maximum current in the coil.

Methodology and experimental tests

The element that was studied was the suspension for a car seat, equipped with a magnetorheological damper (Lord RD-1005-3) (Figure 1, Table 1). The damper is a monotube shock absorber filled with nitrogen gas and it has a high compression ratio. During the movement of the piston, the magnetorheological fluid passes from one chamber of the damper to the other through small holes in the piston that are surrounded by the solenoid coils. By controlling the current flowing through the coil by means of a control system, the value of the magnetic field strength can be changed, resulting in a change in the viscosity of the fluid, which in turn results in a change in the damping force. In addition, a gas accumulator is placed in the vibration damper, which compensates for the change in the volume of fluid caused by the presence of a piston rod that moves the piston. The damping element is mounted in the seat's suspension in such a way that, by changing the damping force, it is possible to affect the vibrations that are transferred from the test station's platform to the car seat.

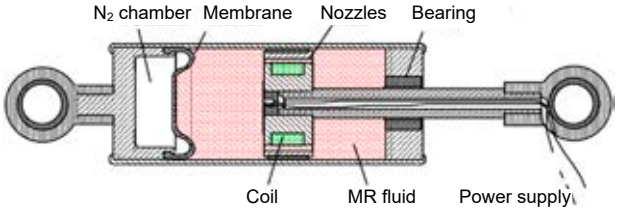

Figure 1. Structure of the damper (Truong & Ahn, 2012)

Table 1. Technical specification of the damper (MR RD1005-3) (Truong & Ahn, 2012)

Parameter	Value
Length of the retracted piston rod, mm	155
Maximum length of the piston rod, mm	208
Diameter of the body, mm	41.4
Diameter of the shaft, mm	10
Mass, g	800
Electrical characteristics:	
Maximum input current, A	2
Input voltage, V DC	12
Resistance	5 Ω at 25°C, 7 Ω at 71°C
Mechanical characteristics:	
Maximum tensile force, N	4448
Maximum operating temperature, °C	171
Response time, ms (depending on the amplifier and power supply)	< 25 (time to reach 90% of the maximum level at the input with a jump from 0 to 1 amps)

The first stage of the research consisted of determining the characteristics of the Lord RD-1005-3 damper. For this purpose, the damper was mounted on a strength test station (Figure 2).

Figure 2. Testing the damper in the test station

The inducer of the testing station generated a kinematic sine induction with constant amplitude (0.04 m) and an induction frequency of 0.5 Hz, 1 Hz, 1.5 Hz, 2 Hz, 2.5 Hz and 3 Hz. These inductions made it possible to determine six graphs of the operation for each of the six current values – the signal controlling the damper (0 mA, 192 mA, 381 mA, 570 mA, 758 mA and 942 mA). The examples of the damper's operation diagrams presented in Figures 3, 4, 5 and 6 confirmed that increasing the current intensity of the input signal, which controlled the damper operation, resulted in an increase of the

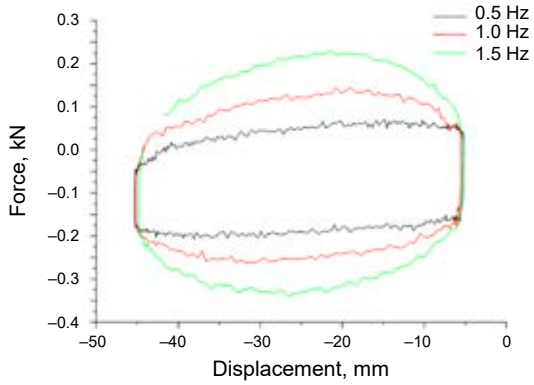

Figure 3. Damping force characteristics as a function of piston stroke for a current of 0 mA

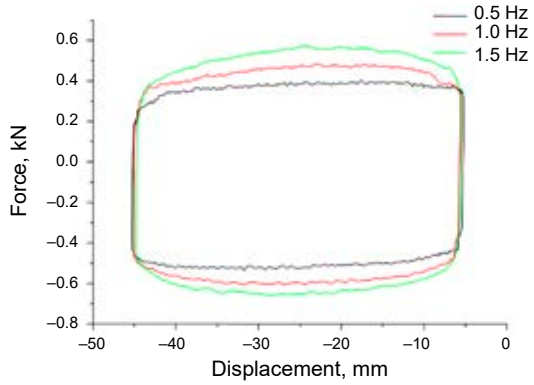

Figure 4. Damping force characteristics as a function of piston stroke for a current of 192 mA

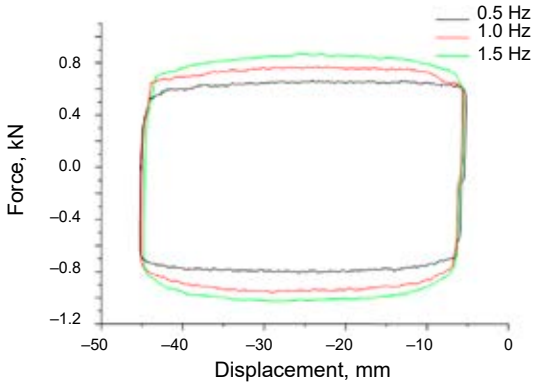

Figure 5. Damping force characteristics as a function of piston stroke for a current of 381 mA

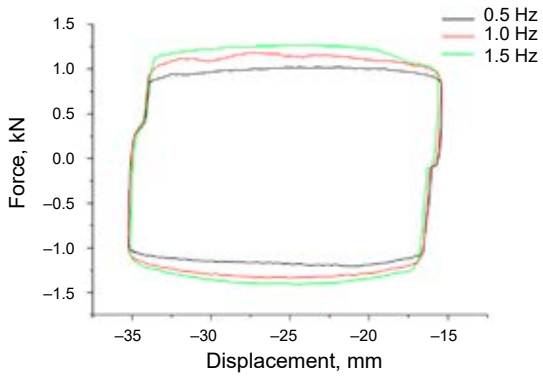

Figure 6. Damping force characteristics as a function of piston stroke for a current of 758 mA

damper's damping force (Osiecki, Gromadowski & Stępiński, 2006).

On the basis of the operation graphs, the damping characteristics were determined; indicating the dependency of the damping force on the piston's displacement velocity. The determined damping characteristics of the damper are presented in Figures 7, 8, 9 and 10.

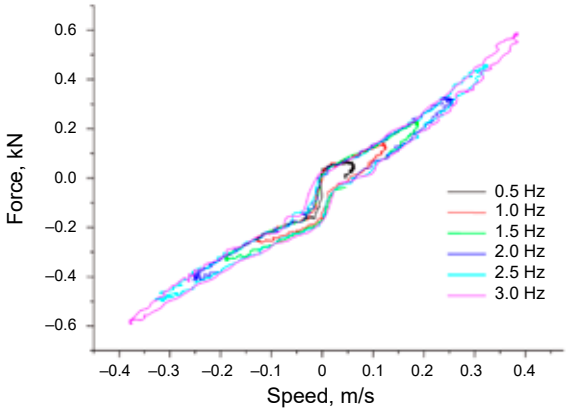

Figure 7. Damping force characteristics as a function of piston displacement velocity for a current of 0 mA

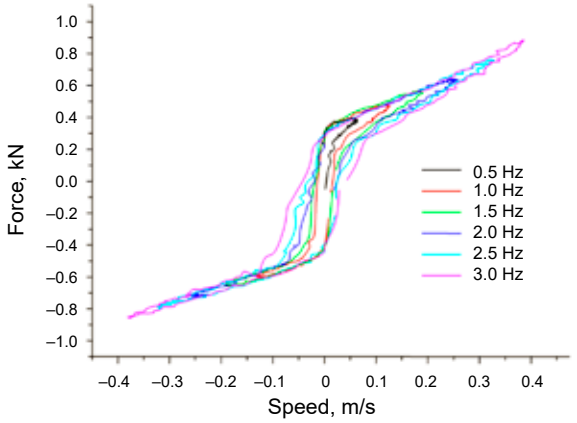

Figure 8. Damping force characteristics as a function of piston displacement velocity for a current of 192 mA

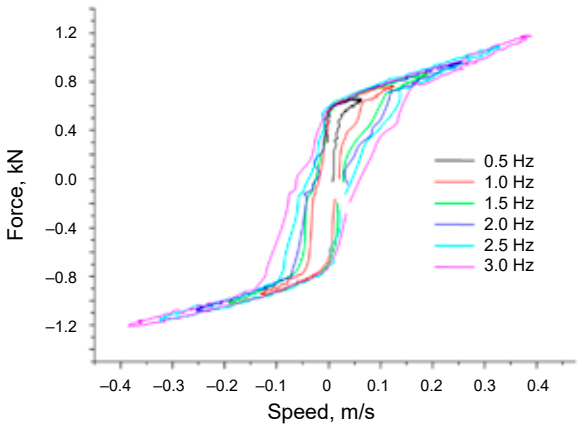

Figure 9. Damping force characteristics as a function of piston displacement velocity for a current of 381 mA

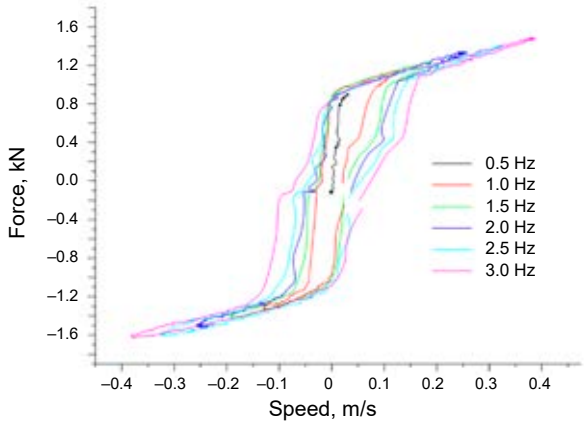

Figure 10. Damping force characteristics as a function of piston displacement velocity for a current of 570 mA

The results of the stationary tests of the damper and their analysis allowed the next stage of the research to be carried out, which was aimed at analyzing how the value of the current that controls the damper affects the travel comfort of the passengers. The tests were carried out at the M.A.S.T. test station shown in Figure 11. Such test stations are built to test the fatigue life of vehicle components and functional tests of complete cars as well as those of individual assemblies or components of vehicles (Gromadowski & Więckowski, 2012; Więckowski, 2015). The test station consists of a movable platform at the top which is connected to a fixed base by a system of six synergic inducers; the inducers generate time-varying displacements and these displacements cause vibrations that affect the tested object. The test station uses measurement and diagnostic equipment based on technology from MTS Systems Corporation.

Figure 11. Testing on the M.A.S.T. test station using a dummy

The conducted tests consisted of the analysis of the impact of a constant acceleration of 4 m/s^2 in the vertical direction on a car seat's suspension equipped with a damper with variable damping characteristics. A dummy of an adult male was placed on the tested seat. In the course of the study, the value of the current of the damper control signal was changed, while the recorded values were the acceleration of the dummy's head and torso, the base of the seat and the top platform of the test station (Zuska & Stańczyk, 2015; Zuska, 2017). The M.A.S.T. test station allowed tests to be carried out simulating mechanical vibrations in the frequency range of 1 to 20 Hz.

Examples of the waveforms of the acceleration recorded at the head and torso of the dummy and on the base of the seat and the top platform for induction frequencies of 4 Hz and 7 Hz are presented in Figures 12, 13 and 14, 15.

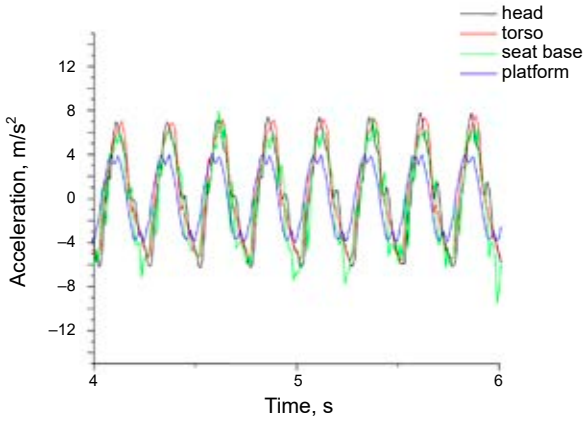

Figure 12. Waveforms of the accelerations recorded for an induction frequency of 4 Hz and a damper controlling current of 0 mA

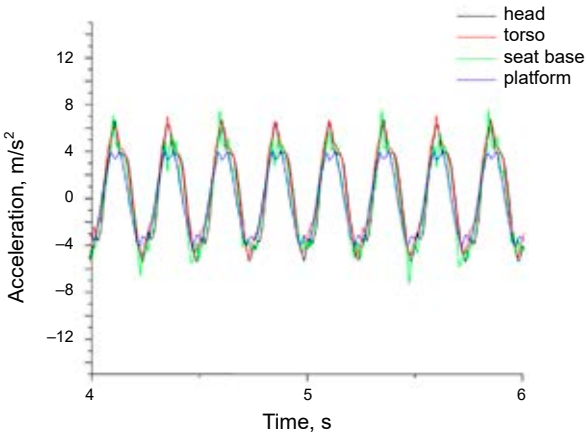

Figure 13. Waveforms of the accelerations recorded for an induction frequency of 4 Hz and a damper controlling current of 381 mA

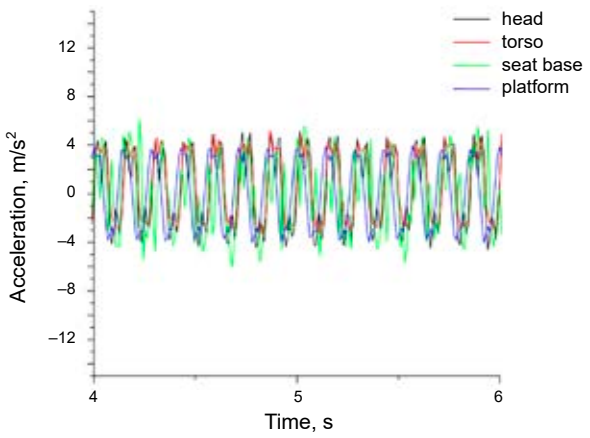

Figure 14. Waveforms of the accelerations recorded for an induction frequency of 7 Hz and a damper controlling current of 0 mA

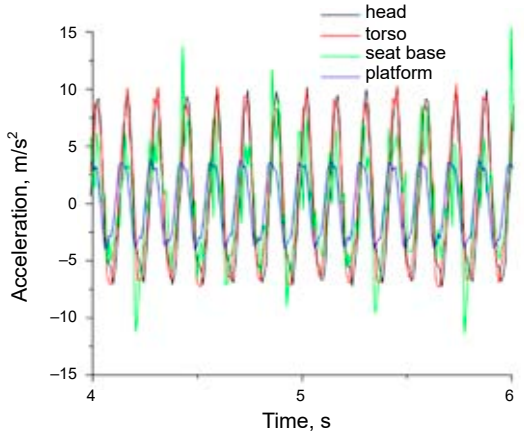

Figure 15. Waveforms of the accelerations recorded for an induction frequency of 7 Hz and a damper controlling current of 381 mA

Based on the recorded waveforms of the accelerations, the RMS indices were determined for the different values of the current controlling the damper's operation, which are presented in Table 2. The impact of the value of the current of the damper control signal on the RMS accelerations, recorded

Table 2. The values of the RMS index of accelerations for induction frequencies in the range 1–20 Hz

0 mA	1 Hz	2 Hz	3 Hz	4 Hz	5 Hz	6 Hz	7 Hz	8 Hz	9 Hz	10 Hz	15 Hz	16 Hz	20 Hz
head	2.00	3.12	3.72	3.63	3.47	2.9	2.7	3.12	3.41	3.07	2.71	2.29	1.46
torso	2.71	3.07	3.41	3.68	3.7	3.2	2.63	2.6	2.65	2.56	1.91	2.26	1.52
seat base	2.88	3.17	3.55	3.11	3.68	3.3	2.73	2.24	2.26	2.19	1.73	2.13	1.6
platform	2.42	2.44	2.39	2.49	2.5	2.43	2.35	2.27	2.2	2.11	1.88	1.83	1.79
192 mA	1 Hz	2 Hz	3 Hz	4 Hz	5 Hz	6 Hz	7 Hz	8 Hz	9 Hz	10 Hz	15 Hz	16 Hz	20 Hz
head	2.70	2.94	3.36	3.28	3.89	4.14	3.8	4.27	4.67	3.97	3.08	2.52	1.69
torso	2.75	2.88	3.12	3.26	3.63	3.93	3.95	4.41	4.67	4.02	2.32	2.49	1.55
seat base	2.91	2.91	3.15	3.11	3.25	3.61	3.3	2.77	3.02	2.96	1.87	1.94	1.64
platform	2.48	2.44	2.45	2.46	2.47	2.34	2.27	2.21	2.21	2.06	1.88	1.95	
381 mA	1 Hz	2 Hz	3 Hz	4 Hz	5 Hz	6 Hz	7 Hz	8 Hz	9 Hz	10 Hz	15 Hz	16 Hz	20 Hz
head	2.68	2.89	3.41	3.31	3.98	4.92	4.76	5.5	5.2	3.85	3.18	2.6	1.95
torso	2.72	2.84	3.05	3.27	3.68	4.39	4.8	5.44	5.07	3.89	2.44	2.4	1.56
seat base	2.88	2.86	3.11	3.1	3.39	4.1	3.91	3.76	3.71	3.13	2.08	1.92	1.7
platform	2.45	2.39	2.38	2.48	2.48	2.41	2.33	2.27	2.24	2.09	1.92	1.84	1.76
570 mA	1 Hz	2 Hz	3 Hz	4 Hz	5 Hz	6 Hz	7 Hz	8 Hz	9 Hz	10 Hz	15 Hz	16 Hz	20 Hz
head	2.69	3.03	3.76	3.32	3.93	4.81	4.82	5.55	5.02	3.88	2.96	2.47	1.86
torso	2.75	2.95	3.31	3.26	3.64	4.5	4.96	5.6	4.89	3.94	2.29	2.3	1.51
seat base	2.87	2.94	3.27	3.06	3.25	4.06	4.43	3.72	3.71	3.22	1.97	2.13	1.61
platform	2.46	2.46	2.55	2.49	2.51	2.43	2.35	2.31	2.17	2.08	1.87	1.77	1.78
758 mA	1 Hz	2 Hz	3 Hz	4 Hz	5 Hz	6 Hz	7 Hz	8 Hz	9 Hz	10 Hz	15 Hz	16 Hz	20 Hz
head	2.74	3.13	3.63	3.31	3.81	4.76	4.9	5.4	5.07	3.89	2.91	2.35	1.79
torso	2.80	2.99	3.21	3.28	3.59	4.58	5.08	5.49	5.03	4.02	2.19	2.16	1.51
seat base	2.92	2.96	3.19	3.2	3.37	4.18	4.23	3.66	3.64	3.53	2.02	2.04	1.6
platform	2.49	2.46	2.44	2.48	2.44	2.46	2.35	2.25	2.17	2.09	1.9	1.79	1.74
947 mA	1 Hz	2 Hz	3 Hz	4 Hz	5 Hz	6 Hz	7 Hz	8 Hz	9 Hz	10 Hz	15 Hz	16 Hz	20 Hz
head	2.76	3.1	3.67	3.27	3.87	4.77	5.24	5.58	5.17	4.13	3.09	2.52	2
torso	2.82	3.01	3.29	3.26	3.67	4.65	5.35	5.66	5.14	4.26	2.27	2.28	1.67
seat base	2.92	2.96	3.3	3.13	3.29	4.29	4.43	4.09	3.55	3.24	2.15	2.1	1.52
platform	2.49	2.47	2.5	2.46	2.49	2.48	2.43	2.31	2.18	2.11	1.92	1.86	1.78

at selected points on the dummy and the base of the seat, at the individual induction frequencies is presented in Figures 16, 17, 18, 19, 20, 21, 22 and 23.

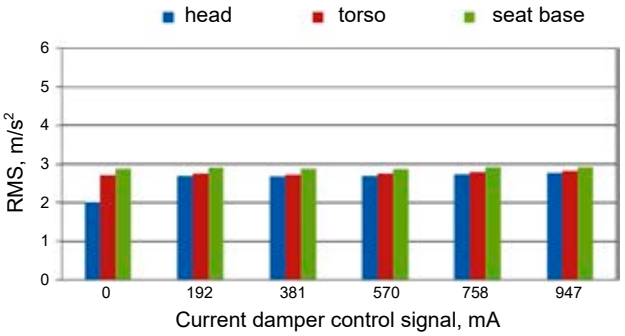

Figure 16. RMS acceleration values for an induction frequency of 1 Hz

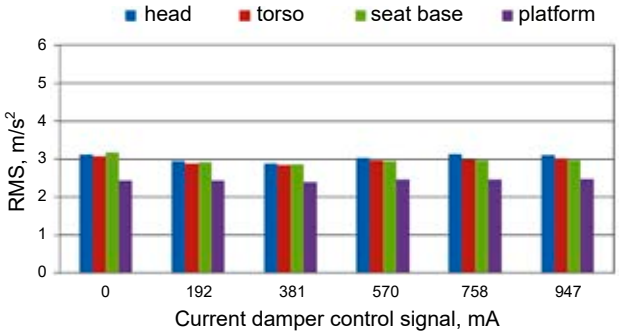

Figure 17. RMS acceleration values for an induction frequency of 2 Hz

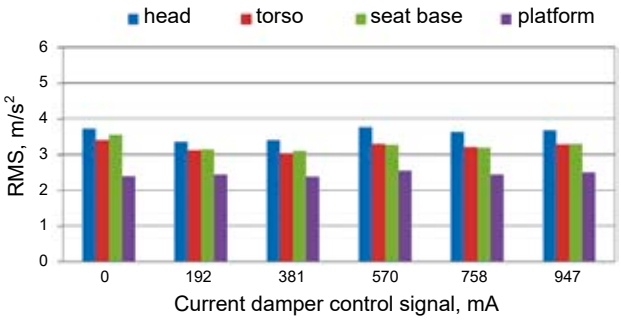

Figure 18. RMS acceleration values for an induction frequency of 3 Hz

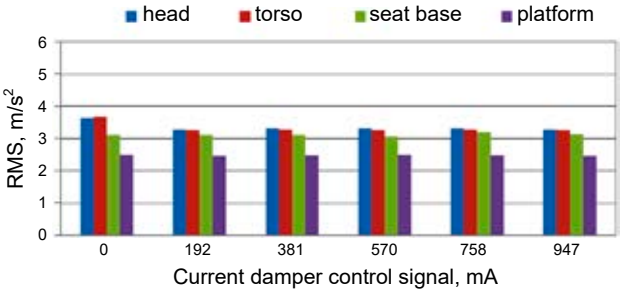

Figure 19. RMS acceleration values for an induction frequency of 4 Hz

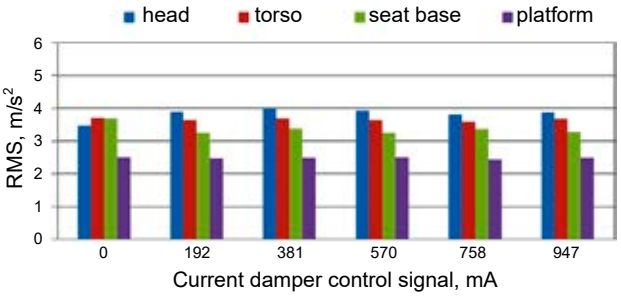

Figure 20. RMS acceleration values for an induction frequency of 5 Hz

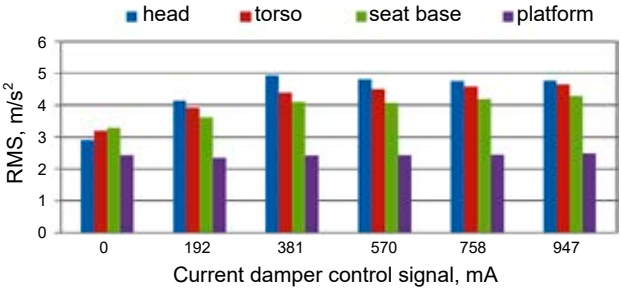

Figure 21. RMS acceleration values for an induction frequency of 6 Hz

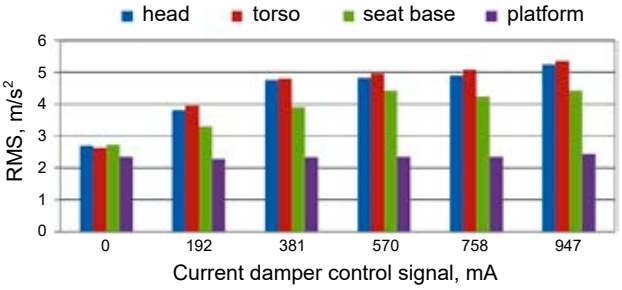

Figure 22. RMS acceleration values for an induction frequency of 7 Hz

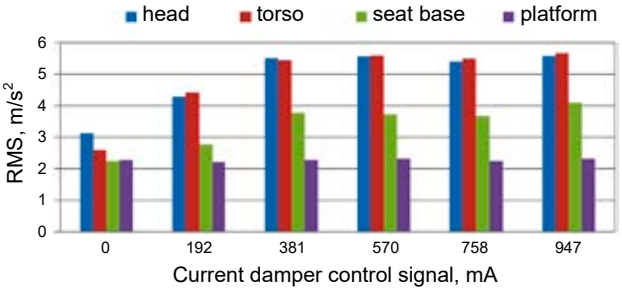

Figure 23. RMS acceleration values for an induction frequency of 8 Hz

Analysis of the test results

After the tests were carried out using the test station, the performance of the damping element installed in the seat's suspension could be evaluated on the basis of the results obtained.

The characteristics (waveform of the accelerations) determined for the selected points on the dummy allowed the influence of the change in the damping force of the damper, mounted in the seat's suspension, on the transmission of vibrations to the human body to be assessed. By comparing the waveforms of the accelerations it can be seen that, for an induction frequency of 4 Hz at different values of the current controlling the damping force, the influence of this force on the values of the obtained acceleration for all of the measurement points is small.

This dependency is noticeable at lower frequencies, from 1 to 4 Hz. The same comparison was made for an induction frequency of 7 Hz, and it was noted that as the damping force increased, so did the acceleration. The highest acceleration values of approximately 10 m/s^2 were recorded at 7 Hz and 8 Hz for values of the damper control signal current of 570 mA, 758 mA and 947 mA. The operation of the damper at these parameters has an adverse effect due to the overlap with the natural frequencies of the system.

The analysis of the RMS index values indicated a disadvantageous influence of the damper's operation mainly in the frequency range of 5 to 10 Hz. When the damper current was 0 mA, the RMS values did not exceed 4 m/s^2. For the other current values, the RMS index reached values in the range of 4–6 m/s^2. In this case, increasing the damper's damping force caused the acceleration amplitudes to increase as well.

Conclusions

The subject of this research fits into the subject matter of the impact of vertical vibrations on people when they are driving a car. The paper presents the results of empirical research on this topic carried out using a test station.

At the turn of the 21st century, there was a step forward in terms of digital signal processing and control technologies. This created new opportunities for active and semi-active vibration damping systems in suspension, e.g. car seats. These technologies can complement traditional passive vibration damping methods, as they are best suited to low-frequency interference in vehicles.

The development of active and semi-active suspension covers interdisciplinary issues, including the theory of car movement, modeling and simulation of car movement, and car dynamic control. This requires combining areas such as mechanics, automation, electronics, computer science and computational techniques, control theory, signal processing and experimental research.

The results of the conducted research have indicated that when the influence of vibration transmission on people while driving is assessed, it is necessary to take into account not only the impact of the value of the current controlling the damper's operation, but also the frequency range of the vibrations transmitted to the vehicle's body. This requires the use of a damper control system combined with time and frequency analysis.

The potential of controlled mechanical vibration damping systems in vehicles are an area which has been known about for decades. However, widespread implementation of controlled suspension systems has become possible relatively recently with the development of cheap processors.

References

1. Islam, M.A., Ahn, K.K. & Truong, D.Q. (2009) Modeling of a magneto-rheological (MR) fluid damper using a self-tuning fuzzy mechanism. *Journal of Mechanical Science and Technology* 23 (5), pp. 1485–1499.
2. Truong, D.Q. & Ahn, K.K. (2012) MR Fluid Damper and Its Application to Force Sensorless Damping Control System. In: G. Berselli, R. Vertechy and G. Vassura (Eds) *Smart Actuation and Sensing Systems – Recent Advances and Future Challenges*. IntechOpen.
3. Osiecki, J., Gromadowski, T. & Stępiński, B. (2006) *Badania pojazdów samochodowych i ich zespołów na symulacyjnych stanowiskach badawczych*. Warszawa: Przemysłowy Instytut Motoryzacji.
4. Więckowski, D. (2015) Research of vertical dynamics of a vehicle on a road simulator test bench– example of comparison and signal evaluation. *Zeszyty Naukowe Wyższej Szkoły Oficerskiej Sił Powietrznych* 3, pp. 137–146 (in Polish).
5. Gromadowski, T. & Więckowski, D. (2012) Analiza drgań pionowych oddziaływujących na dziecko w samochodzie z zastosowaniem wymuszenia sygnałem białego szumu. *Postępy Nauki i Techniki* (*Advances in Science and Technology*) 14, pp. 83–94, Politechnika Lubelska.
6. Gromadowski, T.M., Osiecki, J.W. & Stępiński, B.S. (2001) *Redukcja drgań wybranych modeli pionowej dynamiki samochodu. Opracowanie Problemowe nr BLY.001.01N*. Warszawa: Przemysłowy Instytut Motoryzacji.
7. Gromadowski, T.M., Osiecki, J.W. & Stępiński B.S. (1992) *Eksperymentalne badanie skuteczności aktywnej wibroizolacji fizycznego modelu samochodu*. I Szkoła: Metody Aktywne Redukcji Drgań i Hałasu, Kraków, Wyd. AGH, pp. 51–55.
8. Wu, X., Rakheja, S. & Boileau, P.E. (1998) Study of human-seat interface pressure distribution under vertical vibration. *International Journal of Industrial Ergonomics* 21, pp. 433–449.
9. Ślaski, G., Dąbrowski, K. & Więckowski, D. (2018) Adjustable shock absorber characteristics testing and modelling. *IOP Conference Series: Materials Science and Engineering* 421 pp. 022039-1–022039-10.

10. Jaśkiewicz, M. & Więckowski, D. (2018) Rozwiązania konstrukcyjne aktywnych zawieszeń stosowanych w pojazdach. *Autobusy – Technika, Eksploatacja, Systemy Transportowe* 19, 9, pp. 225–229 (in Polish).
11. Zuska, A. & Stańczyk, T.L. (2015) Analysis of the impact of selected anthropometric parameters on the propagation of vertical vibration in the body of a seated person (driver). *Journal of Vibroengineering* 17, 7, pp. 3936–3948.
12. Zuska, A. & Stańczyk, T.L. (2015) Application of anthropodynamic dummies for evaluating the impact of vehicle seat vibrations upon human body. *Journal of Theoretical and Applied Mechanics* 54, 4, pp. 1029–1039.
13. Zuska, A. (2017) Educational stand for presentation of the vibration propagation in the sitting human (vehicle driver) body. *General and Professional Education* 4, pp. 63–70 (in Polish).